The Rapid Size- and Shape-Controlled Continuous Hydrothermal Synthesis of Metal Sulphide Nanomaterials.

Peter W. Dunne, Chris L. Starkey, Miquel Gimeno-Fabra and Edward H. Lester.*

Department of Chemical and Environmental Engineering, University of Nottingham, University Park, Nottingham, NG7 2RD, UK.

E-mail: Edward.Lester@nottingham.ac.uk; Tel: +44 (0)1159 514974

Experimental Details

Table S1. Details of syntheses performed. Method A used mixed solutions of metal salt and thiourea as the cold stream. In Method B the thiourea solution was the preheated downflow and the metal salt solution was the unheated upflow.

		Concentration (mol L-1)		Flow rate (mL min^{-1})		Temperature (°C)			
Target	Method	$[M^{x+}]$	[Thiourea]	Preheated	Cold	T_{set}	T_1	T_2	Product
ZnS	A	0.05	0.1	20	10	400	408	300	ZnS
	B	0.025	0.025	20	10	250	245	157	ZnS
	B	0.025	0.025	20	10	300	293	191	ZnS
	B	0.025	0.025	20	10	350	348	246	ZnS
	B	0.025	0.025	20	10	400	393	326	ZnS
CdS	A	0.05	0.1	20	10	400	410	302	CdS
	B	0.025	0.025	20	10	250	245	163	CdS
	B	0.025	0.025	20	10	300	298	194	CdS
	B	0.025	0.025	20	10	350	347	239	CdS
	B	0.025	0.025	20	10	400	392	360	CdS
PbS	A	0.05	0.1	20	10	400	408	300	$PbS/PbSO_4$
	B	0.025	0.025	20	10	250	243	155	PbS
	B	0.025	0.025	20	10	300	292	187	PbS
CuS	A	0.025	0.05	20	10	400	385	365	CuS/Cu_9S_5*
	B	0.025	0.025	20	10	250	243	155	CuSCN
	B	0.025	0.025	20	10	300	295	187	CuS
$Fe_{(1-x)}S$	A	0.025	0.05	20	10	400	401	365	$Fe_{(1-x)}S$
	B	0.025	0.025	20	10	250	247	158	FeOOH
	B	0.025	0.025	20	10	300	292	192	FeOOH
	B	0.025	0.025	20	10	350	343	236	FeOOH
	B	0.025	0.025	20	10	400	389	340	$Fe_{(1-x)}S$
Bi_2S_3	A	0.025	0.075	20	10	400	400	351	$Bi_2S_3/Bi_2O_2SO_4$
	B	0.025	0.3	5	10	300	263	93	Bi_2S_3*
	B	0.0125	0.15	5	10	250	227	89	Bi_2S_3

T_{set} = Set temperature of the preheater.

T_1 = Temperature of the preheated stream measured immediately after the heater.

T_2 = Temperature measured post-mixing.

*Caused the rig to block.

Refinement Details

Reitveld refinements were performed on all zinc and cadmium sulphide samples to determine phase composition and crystallite diameters. The GSAS suite within EXPGUI was used for all refinements. The general procedure for the performed refinements follows. Initial models for zinc sulphide were the standard sphalerite and wurtzite structures, ICDD 067790 and 067777, and ICDD 067789 and 060629, for the cubic and hexagonal phases of cadmium sulphide, respectively. In all cases standard Le Bail fits were performed to obtain reasonable starting parameters. Profile parameters were refined initially, until convergence was achieved. Unit cell parameters were then allowed to refine; however in each case they did not deviate significantly from the starting values, and these are the values reported here. The parameters obtained by the Le Bail fits were used as starting values for Reitveld refinements. Scale factors and phase compositions were refined first, followed by further refinement of the profile parameters, which typically did not refine away from those obtained by the Le Bail fits. The refined scale factors and phase composition values were used to determine the phase percentages, and crystallite diameters were calculated from the Lorentzian broadening parameters.

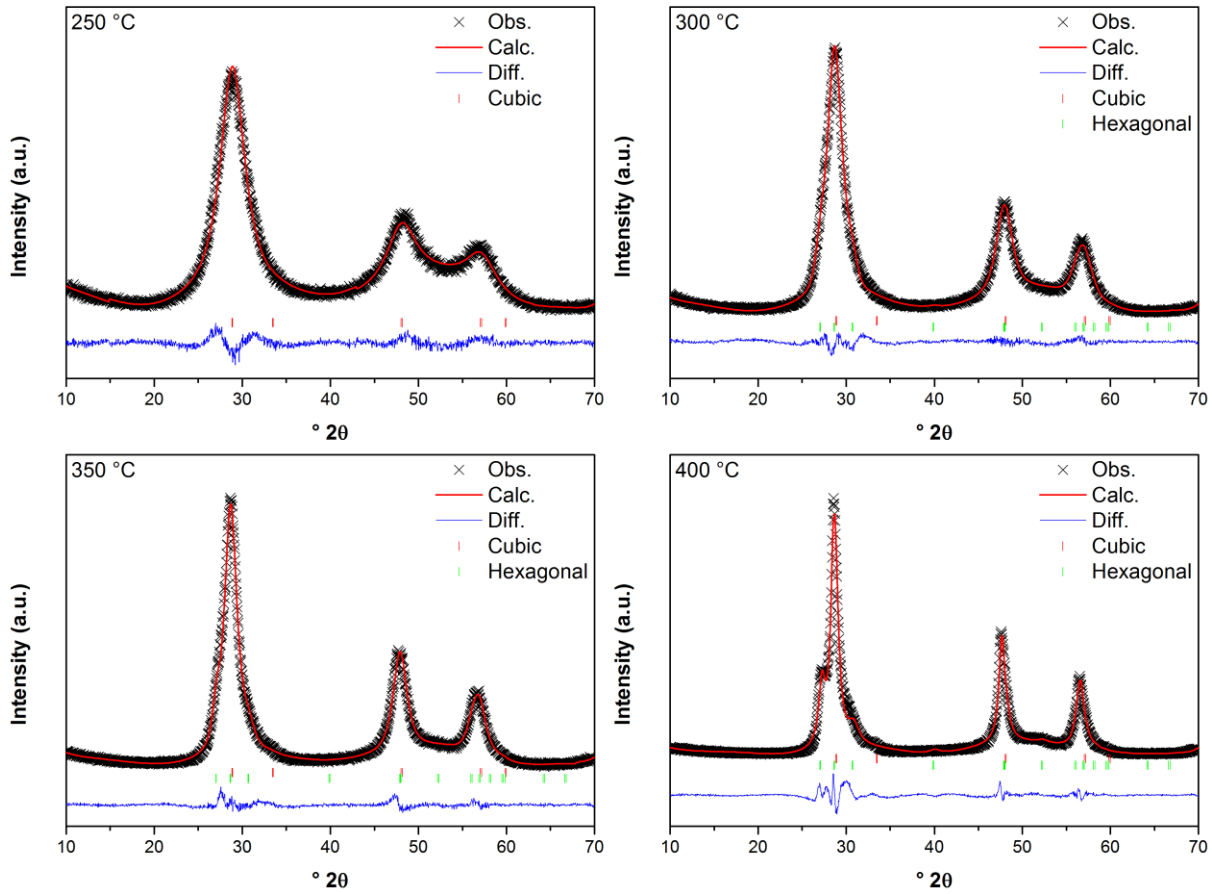

Figure S1. Results of Reitveld refinements on the XRD patterns of ZnS samples prepared at the indicated temperatures fitted with cubic ($F\bar{4}3m$, a = 5.3656 Å) and hexagonal (P63mc, a = 3.7846 Å, c = 6.2089 Å) phases.

It should be noted that the fits in the region of the cubic (111) and hexagonal (002) peaks are somewhat poor and this is thought to be due to stacking faults, the detailed modeling of which is beyond the scope of this work.

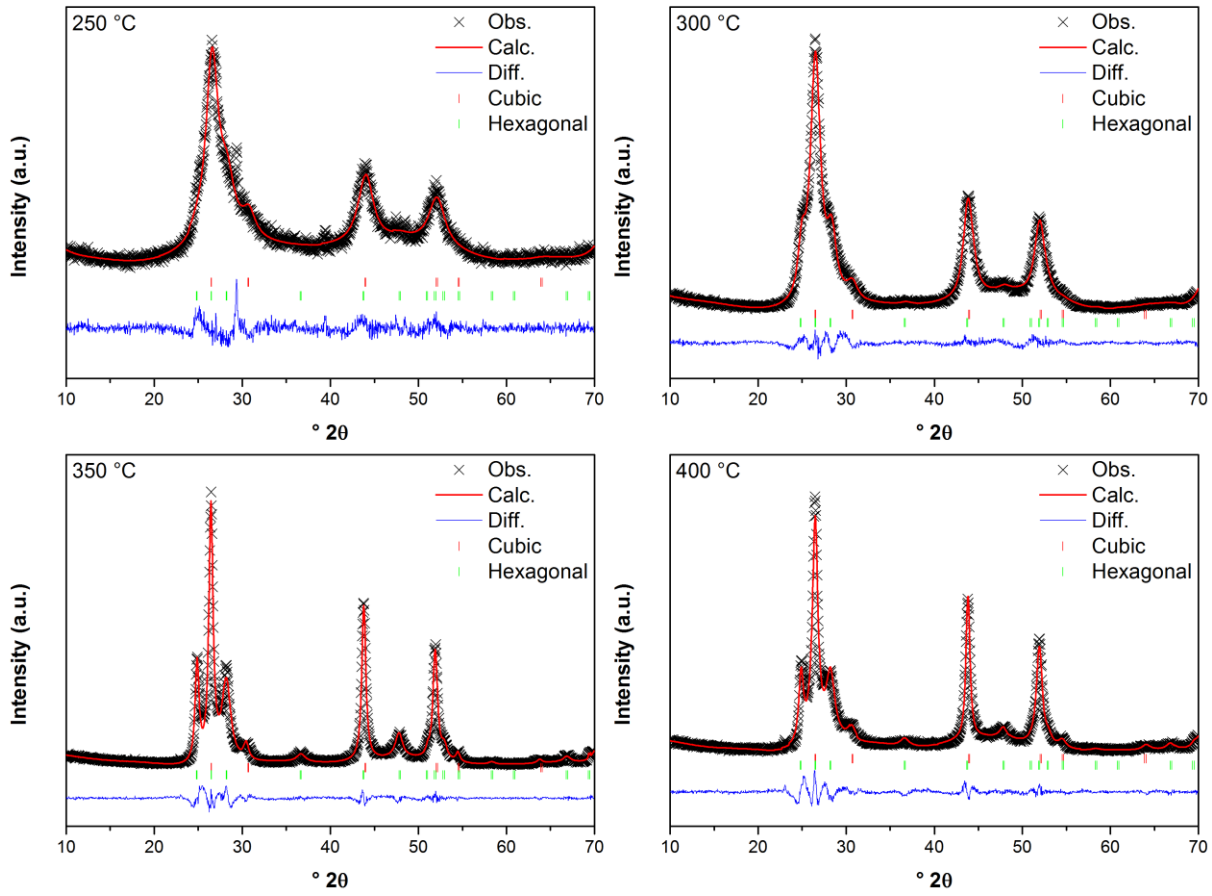

Figure S2. Results of Reitveld refinements on the XRD patterns of CdS samples prepared at the indicated temperatures fitted with cubic ($F\bar{4}3m$, a = 5.8365 Å) and hexagonal ($P6_3mc$, a = 4.1361 Å, c = 6.7222 Å) phases.

It has previously been suggested that similar CdS XRD patterns to those obtained here could be refined as pure hexagonal phase crystallites with cylindrical and spherical morphologies;[1] however these authors disregarded a minor peak at ~31 °2θ arising from the (200) plane of the cubic phase and had to apply a very large number of parameters to obtain their fits. In the case of the cadmium sulphide where there is good separation between the (100) hexagonal peak and the overlapping (002) hexagonal and cubic (111) peaks the refined phase percentages were validated using the formula proposed by Short and Steward:[2]

$$\frac{I_{(100)}}{I_{(002+111)}} = \left(\frac{H}{1.96 - 0.96H}\right)$$

where *I* represents the integrated intensity of the indicated Bragg diffraction peaks and *H* is the hexagonal phase content. The crystallite sizes of the hexagonal phase from Reitveld refinement in the cadmium sulphide samples were also confirmed by single peak fitting of the relatively isolated (100) and (101) peaks using Xfit (the Method B 250 °C sample was excluded from this due to the overlap of the very broad peaks). Similarly the Xfit full-profile fit of the pure sphalerite phase ZnS prepared by Method B at 250 °C gave crystallite diameters in agreement with those obtained from the refined line broadening. This suggests that the results from refinements are quite reasonable.

Fluorescence of ZnS

The fluorescence spectra of all ZnS samples prepared by both methods were recorded using a Flexstation II fluorimeter from Molecular Devices. Samples were prepared by redispersing the dried powder in water at approx. 0.1% (wt/v) and sonicating for 10 to 15 minutes immediately prior to measurement. The fluorescence spectra at excitation wavelengths of 370 nm and 290 nm are shown in Figure S3. At an excitation of 370 nm all samples show the typical self-activated blue luminescence band of ZnS centred around 440 nm. The sample prepared by Method A also shows a strong emission at 590 nm. This was found to be coupled with an excitation band at 290 nm, and excitation at this wavelength gives high intensity fluorescence at 590 nm. Fluorescence bands in this region are commonly observed in Mn^{2+} doped ZnS; however all our samples were prepared from identical sources and no evidence for the presence of manganese has been found in any sample. Similar emissions have previously been reported for ZnS nanobelts and attributed to Mn^{2+} contamination.[3, 4] These authors also reported EDX and TEM results which suggested their product was highly pure. That there is no trace of this orange luminescence in our samples prepared by Method B indicates that this may be a result of the significant twinning observed in the Method A sample. The twinning and intergrowth of the sphalerite and wurtzite phases is likely to induce a variety of defects, from the observable stacking faults to more subtle point defects. It is also possible that surface elemental sulphur species may be generated in this system, which has been implicated as a likely source of similar fluorescent bands in ZnS nanobelts.[5] We posit that it is these defects which are the source of this fluorescence band. Further investigation will be required to confirm or disprove this supposition, however.

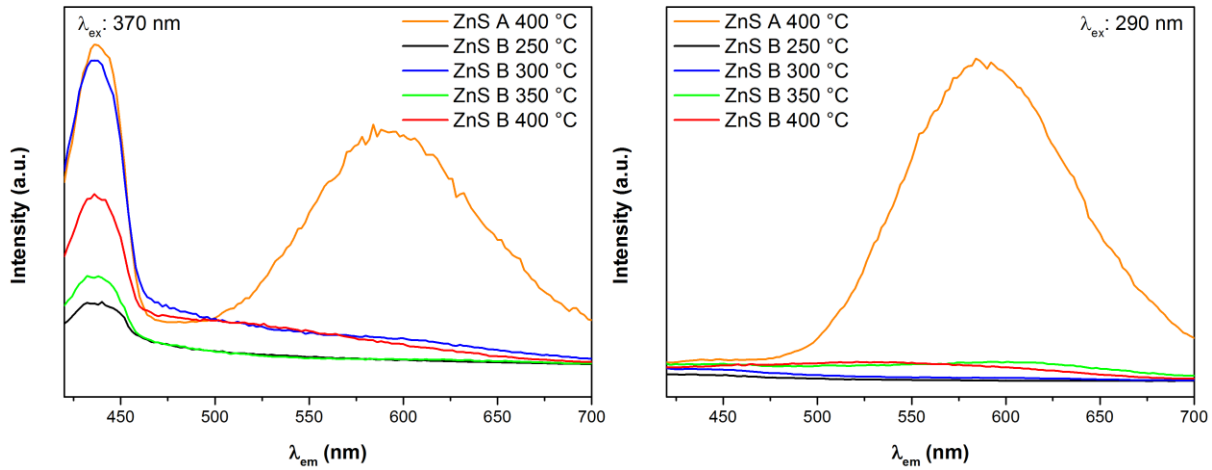

Figure S3. Fluorescence spectra of ZnS samples prepared by Method A and Method B at the temperatures shown with an excitation wavelength of 370 nm (left) and 290 nm (right).

$PbSO_4$

Efforts to synthesise lead sulphide by Method A and Method B at high temperatures typically resulted in white/grey powders being obtained. These were identified as containing lead sulphate as a major phase, as shown in Figure S4 for a Method A sample. This is thought to be due to the oxidation of lead sulphide in the presence of nitrate ions from the lead nitrate precursor and the high temperatures. It was found that even under ambient conditions that the pure lead sulphide formed by Method B at lower temperatures oxidised over time and had to be quickly removed from the acidic supernatant to prevent its transformation to lead sulphate.

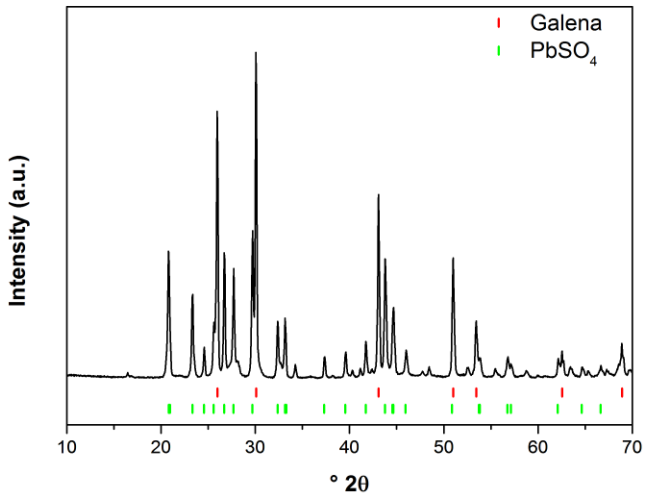

Figure S4. The XRD pattern of the product obtained from the attempted synthesis of PbS by Method A at 400 °C. The product consists of both PbS (galena) and $PbSO_4$.

CuS

Figure S5 shows the XRD pattern and TEM images of the attempted synthesis of copper sulphide by Method A. It is known that covellite phase CuS is the likely product based on the results from Method B; however the low melting and decomposition temperature of covellite resulted in blocking of the rig at high temperatures. The product of the high temperature Method A reaction contains poorly crystalline covellite and more crystalline digenite – a decomposition product of covellite.

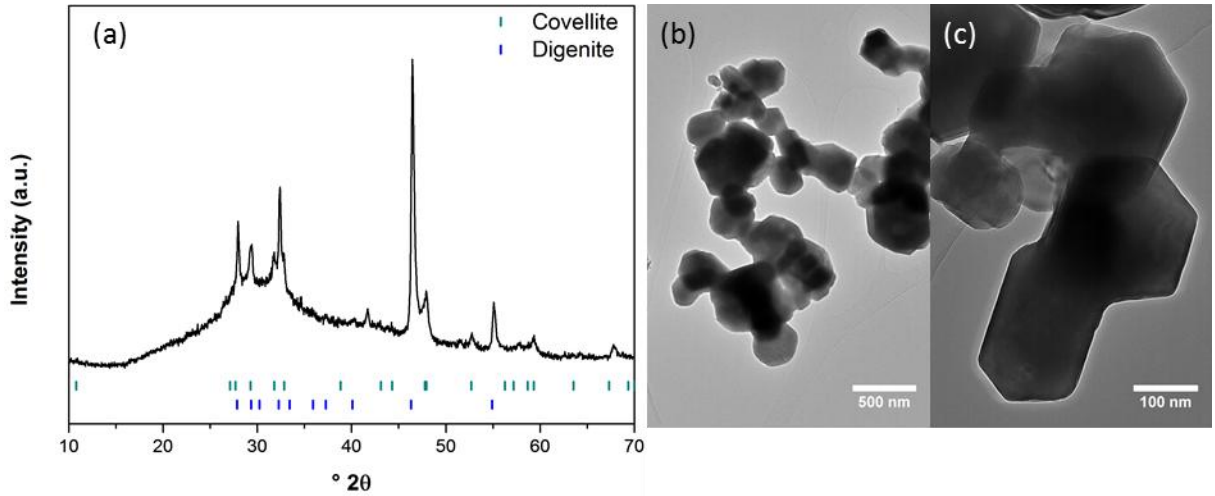

Figure S5. XRD pattern (a) and TEM images (b & c) of the product obtained from the attempted CuS synthesis by Method A.

The white product of the copper nitrate/thiourea reaction by Method B at 250 °C is revealed by XRD to be pure copper thiocyanate.

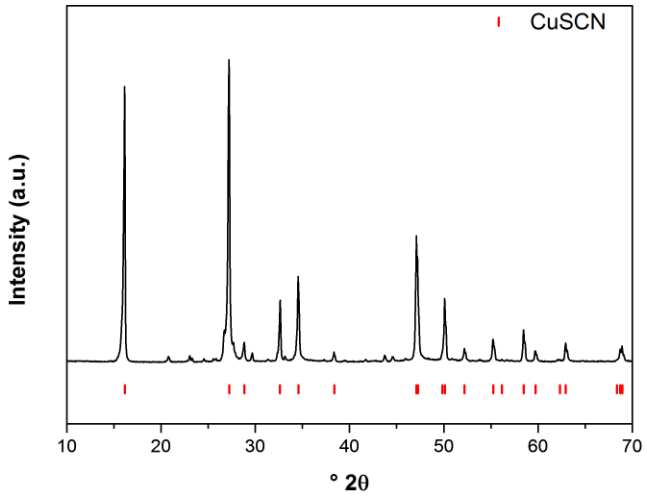

Figure S6. The XRD pattern of copper thiocyantae obtained from the attempted synthesis of CuS by Method B at 250 °C.

The pure covellite phase copper sulphide obtained by Method B at a synthesis temperature of 350 °C was revealed to consist of stacked nanoplatelets. The relationship of these particle morphologies to the crystal structure of covellite is highlighted in Figure S7.

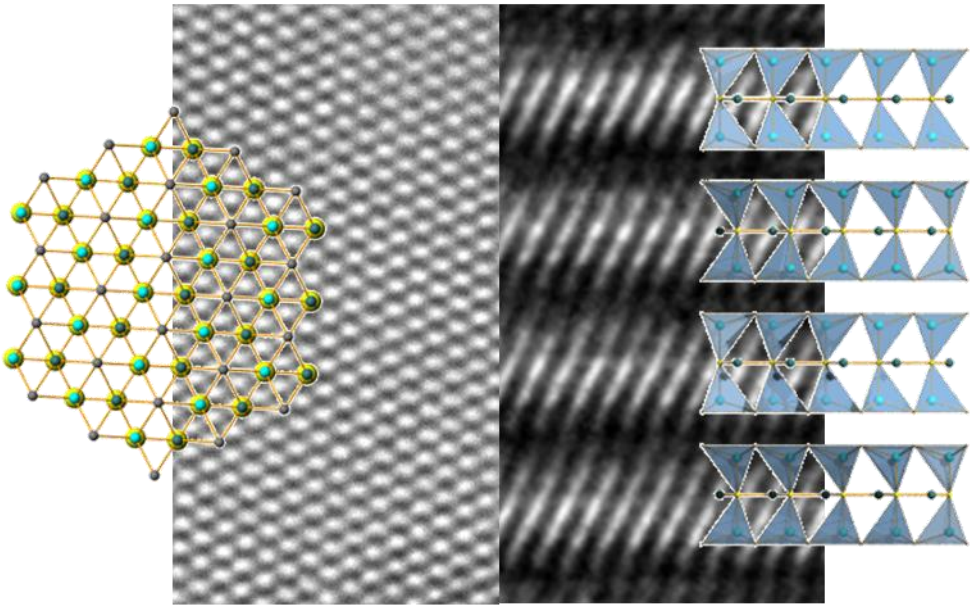

Figure S7. HRTEM images of a single layered hexagonal nanoplatelet with the covellite structure overlaid viewed along the c-axis (left), and an edge on view of stacked platelets compared to 4 stacked "tetrahedron bilayers" (two unit cells in the c-direction) of the covellite structure viewed along the (110) axis (right).

$Fe_{(1-x)}S$ Method B

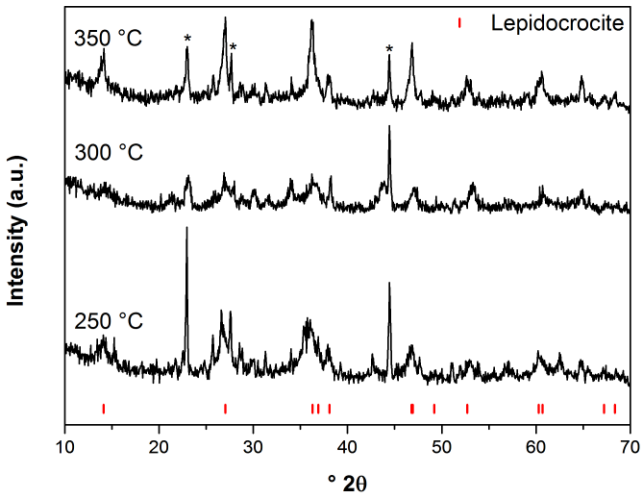

Figure S8. XRD patterns of the products obtained from the synthesis of iron sulphide by Method B at 250 °C, 300 °C and 350 °C. These products were initially obtained as black suspensions, as expected for the synthesis of $Fe_{(1-x)}S$; however they degraded almost immediately on leaving the reactor to give an orange material identified as lepidocrocite, γ-FeOOH.

$Bi_2O_2SO_4$

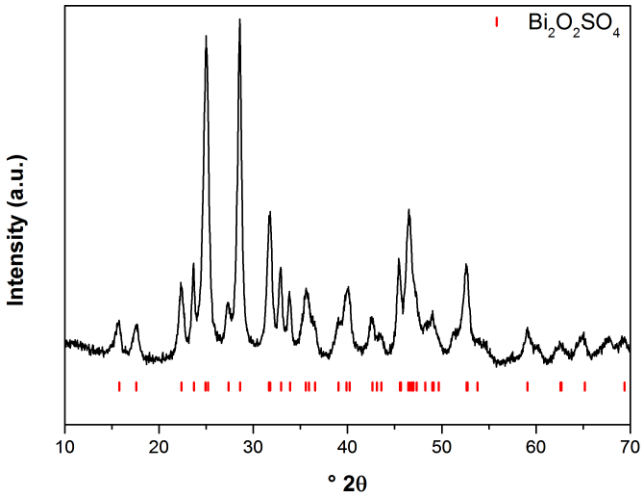

Figure S9. XRD pattern of a typical product obtained from a synthesis of Bi_2S_3 under normal conditions, identified as $Bi_2O_2SO_4$.

References

1. S. R. Aghdaee and V. Soleimanian, J. Cryst. Growth, 2012, 341, 66-71.
2. M. A. Short and E. G. Steward, Am. Mineral., 1959, 44, 189-193.
3. Y.-C. Zhu, Y. Bando and D.-F. Xue, Appl. Phys. Lett., 2003, 82, 1769.
4. D. Denzler, M. Olschweski and K. Sattler, J. Appl. Phys., 1998, 84, 2841-2845.
5. C. Ye, X. Fang, G. Li and L. Zhang, Appl. Phys. Lett., 2004, 85, 3035-3037.